Lab on a Chip

PAPER

View Article Online
View Journal

Cite this: DOI: 10.1039/d5lc00512d

Benchmarking microfluidic and immunomagnetic platforms for isolating circulating tumor cells in pancreatic cancer

Celine Macaraniag,[a] Ifra Khan,[a] Alexandra Barabanova,[b] Valentina Valle,[c] Jian Zhou,[de] Pier C. Giulianotti,[c] Alain Borgeat,[cf] Gina Votta-Velis *[bcg] and Ian Papautsky *[ag]

Pancreatic ductal adenocarcinoma (PDAC) is the fourth leading cause of cancer-related mortality in the US., with poor prognosis due to late-stage diagnosis and high recurrence rates following surgery. Circulating tumor cells (CTCs) are thought to contribute to post-surgical metastasis, while circulating epithelial cells (CECs) have been detected in up to 33% of patients with premalignant pancreatic cysts, offering a potential window for early intervention. Despite their promise as prognostic biomarkers, the clinical utility of CTCs and CECs in pancreatic cancer remains underexplored. Microfluidic technologies offer label-free isolation of rare cells, but few have been benchmarked against clinically validated systems. In this study, we conducted a direct comparison of our inertial microfluidic system with a widely used immunomagnetic negative selection platform (EasySep™). Using matched experimental conditions, we quantified target cell recovery and enrichment to evaluate performance. The inertial microfluidic system demonstrated higher recovery and enrichment, particularly at low cell concentrations, compared to EasySep™, supporting its potential for clinical translation. These findings highlight the advantages of label-free microfluidic isolation and its promise for early detection, prognostic assessment, and therapeutic monitoring in pancreatic cancer.

Received 23rd May 2025,
Accepted 25th July 2025

DOI: 10.1039/d5lc00512d

rsc.li/loc

Introduction

Pancreatic ductal adenocarcinoma (PDAC) is associated with a grim prognosis and ranks as the fourth leading cause of cancer-related mortality in the US.[1] The median overall survival for patients diagnosed with PDAC ranges from 5 to 8 months.[2] A major contributor to this high mortality rate is the fact that PDAC is typically diagnosed at an advanced stage, often presenting with either metastatic or locally advanced disease. Surgical resection remains the primary treatment intervention, despite only a minority of patients qualifying for primary surgical intervention and systemic chemotherapy.[1] Among those who undergo successful resection, disease recurrence occurs in about 70% of cases.[2] These factors underscore the significant clinical challenges poised by PDAC and highlight the need for a multidisciplinary approach to both prognostic assessment and therapeutic management.

Given the high metastatic propensity of PDAC, one promising prognostic strategy involved enrichment and analysis of circulating tumor cells (CTCs). These rare cells are shed into the circulation either by the primary tumors or during surgical manipulation.[3] CTCs are increasingly recognized as potential indicators of disease recurrence and overall survival following initial therapy or surgical resection.[4–7] Their presence has been correlated with poor prognosis in both early and late stages of PDAC.[1] Moreover, circulating epithelial cells (CECs) have been detected in premalignant stages of the disease. Notably, up to 33% of patients with precancerous cystic lesions (such as intraductal papillary mucinous neoplasms or IPMNs) exhibit CECs prior to a clinical cancer diagnosis.[8] In PDAC, CTCs may enter the circulation either after undergoing partial epithelial-to-mesenchymal transition (EMT) or in a mesenchymal state, later reverting to an epithelial phenotype.[9] Consequently, the detection and enumeration of CTCs and CECs may serve as a valuable tools for early

[a] Department of Biomedical Engineering, University of Illinois Chicago, Chicago, IL, USA
[b] Department of Anesthesiology, University of Illinois Chicago, Chicago, IL, USA
[c] Department of Surgery, University of Illinois Chicago, Chicago, IL, USA
[d] Department of Cardiovascular and Thoracic Surgery, Rush University Medical Center, Chicago, IL, USA
[e] Department of Anatomy and Cell Biology, Rush University Medical Center, Chicago, IL, USA
[f] Department of Anesthesiology, Balgrist University Hospital Zurich, Zurich, Switzerland
[g] University of Illinois Cancer Center, Chicago, IL, USA

diagnosis, risk stratification, and prognostic assessment in PDAC,[5] with the potential to inform clinical decision making and improve patient outcomes.

Various strategies for rare cell enrichment have been developed to enhance the identification and isolation of CECs and CTCs since their detection rate in pancreatic cancer patients is relatively low.[4,5] These approaches include both physical and immunological separation techniques.[10] Immunoaffinity-based methods target specific surface markers, either by depleting non-target cells (negative enrichment) or capturing target cells (positive enrichment).[10,11] Positive enrichment typically isolates EpCAM-positive cells, while negative enrichment removes hematopoietic cells by targeting surface markers such as CD45, using immunomagnetic or immunodensity-based methods.[13] Commercial systems such as Dynabeads™ and EasySep™ use magnetic beads conjugated with antibodies to bind and remove undesired cells. RosetteSep™ uses an immunodensity-based approach, using antibodies to alter the buoyancy of undesired cells, which are then removed through density gradient centrifugation followed by Cytospin for target cell enumeration.[12] Despite their widespread use in research, these methods face limitations in cell recovery, largely due to the heterogeneity of epithelial marker expression among CECs, particularly in the context of EMT.[9,14,15] In addition, using multiple surface markers to capture diverse CTC populations can significantly increase the cost and complexity of each analysis.

In contrast to immunological approaches, physical enrichment techniques selectively isolate cells based on intrinsic biophysical properties such as size, density, or deformability.[16] These include optical, electrical, acoustic, and mechanical isolation methods.[17] Label-free strategies are particularly advantageous, as they do not depend on surface marker expression,[16] which can vary significantly among CTC populations,[14,18] potentially compromising recovery efficiency. Commercially available label-free platforms such as Parsortix,[19,20] Vortex (VTX-1),[21] and ClearCell® FX[22] use size and deformability-based sorting to achieve high recovery rates. However, these systems have not yet been validated for pancreatic cancer. Microfluidic platforms that have demonstrated success in isolating pancreatic cancer CTCs often incorporate immunocapture techniques to enhance specificity.[18,23–27] Nonetheless, challenges such as heterogeneous surface marker expression,[18,27] limited throughput, and high operational costs have restricted their clinical translation. Among label-free approaches, inertial microfluidic (iMF) systems have emerged as a promising alternative for isolating CTCs based on size differentials. Given that CECs and CTCs are generally larger than most blood cells,[28] iMF devices can exploit this property to enable efficient, high-throughput, and cost-effective rare cell enrichment, making them particularly attractive for applications in PDAC.

In this study, we evaluate the performance of an iMF device in comparison to an affinity-based negative enrichment technique, specifically the EasySep™ immunomagnetic separation system, for the isolation of CTCs and CECs (Fig. 1). We conduct a comparative analysis to assess both target cell recovery and enrichment efficiency between the two platforms. Importantly, neither method relies on cancer cell surface makers, thereby preserving the phenotypic heterogeneity of the isolated cells. To validate the iMF system, we first assessed its ability to recover PANC1 pancreatic cancer cells spiked into healthy blood samples. Subsequently, we applied the device to isolate tumor cells from blood samples obtained from PDAC patients. By quantifying both recovery rates and enrichment, this study aims to demonstrate the utility of microfluidic isolation as a robust and marker-independent approach to rare cell capture in PDAC.

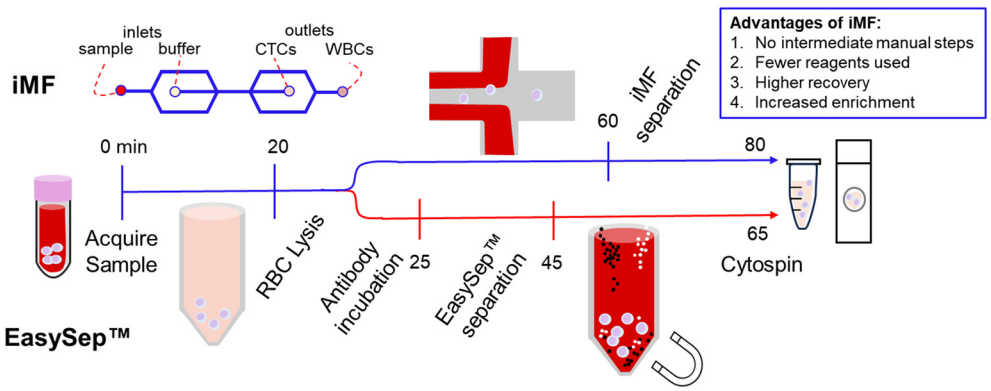

Fig. 1 Workflow for processing a standard 7.5 mL blood sample using microfluidic and immunomagnetic approaches. In the microfluidic workflow, spiked blood is introduced into the inertial microfluidic device, followed by cytocentrifugation and imaging. The processing time for microfluidic separation is volume-dependent and can be shortened for smaller samples; further reductions in processing time are possible by operating multiple devices in parallel. In the immunomagnetic workflow, antibodies are first added to the spiked sample to label unwanted cells. The sample is then placed in a magnetic field, allowing labeled cells to be retained while unlabeled target cells are transferred to a new tube for analysis. Unlike the microfluidic approach, the total processing time for the immunomagnetic method is fixed and independent of sample volume.

Experimental methods

Cell culture

The human pancreatic cancer cell line (PANC1) was obtained from (ATCC, Manassas, Virginia). PANC1 cells were grown at 37 °C with 5% CO_2 to 80% confluency in DMEM (Corning Inc., Corning, NY, USA), 10% (v/v) FBS (GeminiBio Inc., West Sacramento, CA, USA), and 1% (v/v) antibiotic–antimycotic (100×). The adherent cells were dissociated with TrypLE™ Express Enzyme (1×), phenol red (Fisher Scientific, Waltham, MA, USA) and re-suspended in complete media.

Blood sample preparation

Healthy blood was obtained from human volunteers drawn from the left or right forearm. Approximately 6–8 mL blood was collected in EDTA tubes (BD, Franklin Lakes, NJ, USA). RBCs were lysed from blood samples with 10 mL ACK lysing buffer for every 1 mL of blood (KD Medical Inc., Columbia, MD, USA) and incubated at room temperature for 10 min. After lysis, the samples were centrifuged at 300*g* for 5 min and washed with 1× PBS. The blood samples were spiked with 50, 100, and 500 PANC1 cells per 1 mL. PANC1 cells were stained with Hoechst 33342 (ThermoFisher), 1 : 1000 dilution, incubated at room temperature for 15 min, and then washed before spiking into the blood.

For clinical validation, 10 mL blood samples were collected from surgical patients diagnosed with PDAC, NET, or IPMN using K2-EDTA tubes. Blood draws were performed at four time points: pre-operatively and 72 h post-operatively by venipuncture, and intra-operatively and 24 h post-operatively by arterial line. RBCs were lysed using in the same protocol applied to spiked blood samples, as previously described. Following lysis, samples were resuspended in 1× PBS. Isolated cells were subsequently fixed onto slides *via* cytocentrifugation, rendering them non-viable; therefore, cell viability was not assessed.

Microfluidic device fabrication and operation

The iMF device is a straight microchannel (150 μm × 50 μm × 24 mm, $w \times h \times l$) configuration with two inlets and two outlets. The sample is introduced through the first inlet, where it bifurcates into two lateral streams that flow along the channel sidewalls. A buffer solution is introduced through the second inlet, forming a central stream between the sample flows. At the outlet, target cells are collected through the inner outlet, while the outer outlet removes the majority of blood cells. The microchannel was fabricated in polydimethylsiloxane (PDMS) using a dry film master photoresist masters, as we described previously. Dry films (ADEX 50, DJ MicroLaminates Inc., Sudbury, MA, USA) were used to pattern the microchannels on 3″ silicon wafers.[29] The microchannels were then replicated in PDMS (Sylgard 184, Dow Corning, Midland, MI, USA) and bonded to 1″ × 3″ glass slides (Fisher Scientific Inc., Hampton, NH, USA) to form sealed devices following oxygen surface plasma treatment for 20 s (PE-50, Plasma Etch Inc., Carson City, NV, USA). Inlet and outlet ports were manually cored using a biopsy punch with an outer diameter of 1.5 mm (TedPella Inc., Redding, CA, USA).

PANC1 cells were spiked in 1 mL of lysed blood and 1× PBS and used in recovery experiments. The spiked samples flow on both sides of the channel near the wall. Cells will migrate laterally toward the center of the channel, strongly dependent on cell size.[28] This mechanism separates differentially sized cells in a simple straight channel where three flow streams are formed in the main channel, with buffer flow in the middle to collect larger target cells. A 300 μL min^{-1} flow rate is selected to obtain the flow condition of Re = 50, which requires the shortest channel length for focusing. Following microfluidic isolation, the target cells were collected as diluted cell samples, about 1–1.5 mL, in 2 mL microcentrifuge tubes. The collected cell sample was centrifuged at 300*g* for 5 min to remove excess volume and leave ~400 μL. To ensure that as many cells as possible reach the slide, the cytofunnel filter was pre-wetted with 100 μL of 10% FBS–PBS for 5 min in the Cytospin before loading the cell sample.

EasySep™ separation

EasySep™ Direct Human CTC Enrichment Kit (STEMCELL Technologies, Seattle, WA, USA) was used as our immunomagnetic enrichment isolation method. PANC1 cells were spiked in either 1 mL of lysed blood, whole blood, or 1× PBS. With smaller cell spikes, 100 or 50, sample droplets of the predicted spikes were counted in triplets to confirm if spike volumes were accurate. The cell suspension is mixed thoroughly before each use. The spiked samples were added to 15 mL rounded tubes, and 50 μL of the enrichment cocktail was added to the tube and mixed and incubated for 5 min at room temperature. Target cells were isolated according to the manufacturer's protocol. After isolation, cells were suspended in 1× PBS.

Immunostaining and cytocentrifugation

Isolated cells were spun on glass slides using Cytospin 4 (Thermo Fisher Scientific) at 500 rpm for 13 min and fixed with 4% (v/v) paraformaldehyde. Cells on cytospin slides were imaged through an inverted fluorescence microscope (IX83, Olympus) after each separation experiment. For captured CTCs from patient blood, Cytospin slides were immunostained with Ms anti-pan-cytokeratin (CK) antibody, Alexa Fluor® 488, AB277270 (Abcam), Rb anti-CD45 antibody, Alexa Fluor® 647, AB200317 (Abcam) and Hoechst 33342 (ThermoFisher).

Image acquisition and data analysis

The collected cell suspension was centrifuged to count recovery for small cell spikes, and excess liquid was aspirated until 100 μL was left. The remaining 100 μL solution was directly loaded onto a glass slide to count the recovered cells.

For 10 000 cell spikes, recovery was calculated from cytospin slides. The enrichment ratio is defined as the ratio of CTCs to WBCs in the output relative to that in the input.

A high speed camera (FASTCAM Mini AX200, Photron USA Inc.) was used (exposure time: 5 s, frame rate: 250 fps) to image cells flowing inside the microchannel and to image cells flowing within the microchannel in a bright field during large spike cell separation experiments. Image processing and analysis were conducted using ImageJ. Data analysis and graphing were done in Microsoft Excel. Total cell recovery is the number of tumor cells collected after isolation over the total number of cells injected into the device. Total cell recovery is the fraction of the target cells in the target outlet, and the total number of cancer cells spiked into the sample. The adjusted iMF Recovery rate was calculated as the total cell recovery over the cytocentrifugation recovery.

Ethical statement

All procedures involving human participants were conducted in accordance with the ethical standards outlined in 45 CFR 46 of the U.S. Department of Health and Human Services. The study protocol (UIC IRB #2023-0101) adheres to these guidelines and was reviewed and approved by the University of Illinois Chicago Institutional Review Board. Informed consent was obtained from all participants prior to their inclusion in the study.

Results and discussion

Evaluation of cancer cell isolation using an inertial microfluidic device

The sizes of cancer cells and WBCs were first characterized to ensure the iMF device could effectively isolate target cells from a heterogeneous sample. Because cytocentrifugation can compromise cell integrity and distort size measurements (Fig. 2A), all size measurements were performed on cells in suspension, prior to any processing, to maintain measurement accuracy. The average diameters of viable PANC1 cancer cells and WBCs in suspension were 22.1 μm and 8.4 μm, respectively (Fig. 2B). Our previous work[30] has established the iMF device's separation efficiency and defined a cutoff size of 12 μm, the minimum particle size that can be reliably separated from the sample. Since this cutoff is smaller than the average size of PANC1 cells, the device is capable of capturing approx. 99.5% of these cells.[30] To assess whether the separation process affects viability of cells, we evaluated cells post-separation and observed a high relative viability of 95.2 ± 2.6% (Fig. 2C). In contrast, cytocentrifugation resulted in substantial cell death, with viability dropping below 10%. These findings indicate that the iMF device preserves cell viability during separation.

The iMF device employs a multi-flow configuration in which the blood sample is introduced on both sides of a straight microchannel, while a buffer stream flows between the sample streams. In this configuration, cells migrate laterally towards two equilibrium positions located near the center of the channel.[31] Due to their larger size, cancer cells migrate more rapidly to these equilibrium positions compared to smaller cells, such as WBCs, and are consequently collected at the central outlet (Fig. 3A). The effective size cutoff of the device is determined by the length of the downstream channel segment. Following each spiking experiment, pre-stained tumor cells were identified and enumerated *via* microscopy after cytocentrifugation (Fig. 3B). Although some WBC contamination was observed, it did not significantly interfere with the accurate enumeration of tumor cells.

Since RBC lysis was necessary for effective isolation of target cells, it was important to assess whether this step contributed to significant cell loss. To evaluate this, cancer

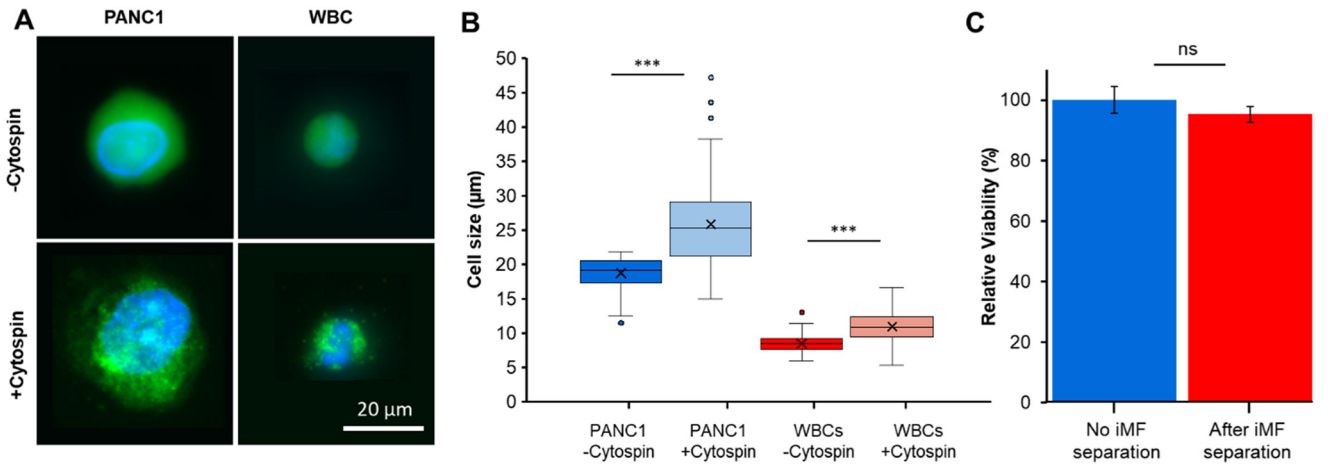

Fig. 2 Characterization of PANC1 cells and WBCs size and viability. A) Fluorescent images of PANC1 cells and WBCs stained with Calcein AM (green) and Hoechst 33342 (blue), imaged in suspension (–Cytospin) and after cytocentrifugation (+Cytospin) on a glass slide. Scale bar: 20 μm. B) Quantitative comparison of cell diameters before and after cytocentrifugation of PANC1 cells and WBCs. Cytospin significantly increased the apparent size of both cell types ($p < 0.001$). C) Viability of PANC1 cells following iMF separation and prior to cytocentrifugation, indicating minimal impact of the microfluidic process on cell integrity.

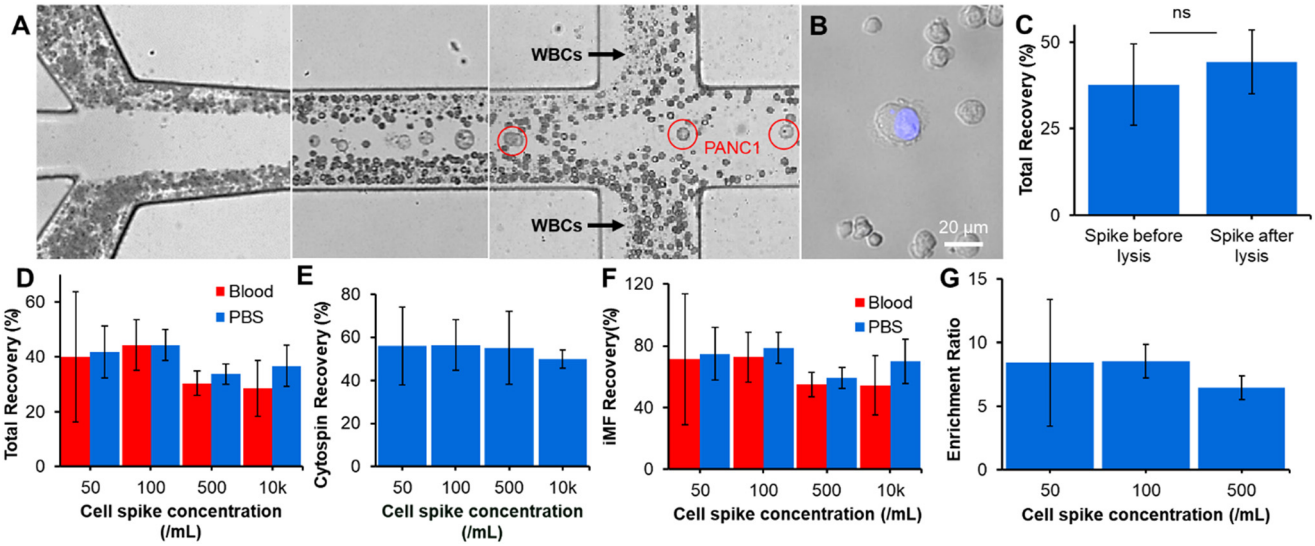

Fig. 3 Performance evaluation of inertial microfluidic (iMF) isolation. A) Microfluidic separation at the outlet, illustrating that target cells (PANC1) migrate to the central collection channel, while the majority WBCs are diverted to the side channels and discarded. B) Representative image of PANC1 cells isolated by iMF and stained with Hoechst 33342. C) Comparison of cell yield from spike-in experiments with PANC1 cells added to blood before *versus* after RBC lysis. D) Total cell yield following iMF separation and cytocentrifugation across different spike-in concentrations. E) Cytospin recovery rates for each spike-in concentration, highlighting cell loss during this step. F) Adjusted microfluidic recovery rates accounting for cytospin cell loss. G) Enrichment ratios following iMF separation at each spike-in concentration, demonstrating consistent performance across input levels.

cell lines were spiked into whole blood either before or after RBC lysis. When spiked prior to lysis, the mean recovery of CTCs from 100-cell spikes was 37.8 ± 11.8%. This was comparable to the recovery of 44.3 ± 9.2% observed when cells were spiked after RBC lysis (Fig. 3C), indicating that the lysis process does not result in substantial cell loss. Spiking cancer cells after lysis also enables direct assessment of the microfluidic device recovery efficiency, independent of upstream sample processing. Given the reported rarity of CTCs in patient samples, approx. 1 CTC per 7.5 mL of blood,[4,6,32] we evaluated device performance across a range of spiked CTC concentrations (50, 100, 500 cells per mL, and 10 000 cells per mL). In blood samples, the total recovery following iMF separation and cytocentrifugation was 40 ± 23.7% (n = 4), 44.3 ± 9.2% (n = 5), and 30.3 ± 4.4% (n = 3) for 50, 100, and 50 cell-spikes, respectively (Fig. 3D). At 10 000 cells per mL, the mean recovery was 28.6 ± 10.2% (n = 3). To determine whether the sample matrix influenced recovery, equivalent spiking experiments were conducted in phosphate-buffered saline (PBS). The mean recovery rates were 41.9 ± 9.4% (n = 4), 44.4 ± 5.6% (n = 4), and 33.8 ± 3.7% (n = 3) for 50, 100, and 500 cell-spikes, respectively, and 36.7 ± 7.5% (n = 3) at 10 000 cell per mL No statistically significant differences were observed between recoveries from blood and PBS, suggesting that the sample medium does not substantially affect the performance of the iMF device.

Our previous work on CTC enrichment from breast cancer samples demonstrated that cytocentrifugation alone can result in 33–45% cell loss.[30] To account for this, we

Table 1 Microfluidic enrichment of spiked pancreatic cancer cells

Isolation type	Key features	Cell type	Spike (cells per mL)	Spiked sample	Recovery (%)	Throughput (mL h^{-1})	Ref.
Microfluidic immunocapture	Antibody-coated micro posts	Capan-1, PANC1, BxPC-3	300	500/mL PBMCs	30–70	1	Thege, *et al.* 2014 (ref. 18)
	Antibody-coated chip (EpCAM)	NB508 (mouse)	5000	2× diluted whole blood	35	1.5	Yu, *et al.* 2014 (ref. 33)
	Antibody-coated micro posts (EpCAM, CD133)	Capan-1, PANC1	1000	Whole blood	73–95	1	Zeinali, *et al.* 2018 (ref. 27)
Microfiltration immunocapture	Lateral microfiltration with immunoaffinity (EpCAM)	L3.6pl	10–10 000	2× diluted whole blood	93.5	3.6	Chen, *et al.* 2020 (ref. 25)
Microfluidic + EasySep™	Magnetic nanobeads coated with EpCAM and vimentin	PANC1	67	4× diluted WBCs	33–82	2	Cha, *et al.* 2023 (ref. 26)
Microfluidic physical isolation	Inertial focusing (multi-flow straight channel)	PANC1	50, 100, 500	4 000 000/mL WBCs	55–78 (29–44 with Cytospin)	6	This work

calculated the adjusted recovery rates of our iMF system by excluding the contribution of cytocentrifugation to total cell loss. In PBS-spiked samples, cytocentrifugation alone yielded recovery rates of 56.0 ± 18.0% (n = 4), 56.4 ± 11.6% (n = 3), 55.2 ± 16.9% (n = 3), and 50.0 ± 4.2% (n = 4) for 50, 100, 500, and 10 000 cell-spike concentrations, respectively (Fig. 3E). By correcting for this loss, the adjusted recovery rates attributable to the iMF device alone were calculated as 74.8 ± 16.9%, 78.7 ± 9.9%, 59.3 ± 6.7%, and 69.9 ± 14.3%, respectively (Fig. 3F). Residual cell loss is likely due to factors such as retention in the waste outlets and losses during post-processing sample transfers. When compared to other microfluidic isolation platforms used for pancreatic cell enrichment,[18,26,33] the iMF device demonstrates comparable or superior recovery rates, particularly at low cell concentrations. Notably, many existing systems rely on immunocapture of EpCAM+ cells and report variable capture efficiencies (Table 1). In some cases, higher recovery rates were reported when enumeration was performed directly within the device, without retrieving the cells.[18,25,27] While this approach may improve recovery, it limits downstream molecular or functional analyses that require cell retrieval.

In addition to recovery, we assessed the enrichment ratio as a unified metric to simultaneously quantify WBC depletion efficiency and overall sample purity. The enrichment ratio, defined as the change in the ratio of target cells to WBCs from the inlet to the outlet, demonstrated consistent performance across a range of spike-in concentrations. Specifically, at spike-in concentrations of 50, 100, and 500 cells per mL, the enrichment ratios were 8.4 ± 5.0, 8.6 ± 1.3, and 6.5 ± 0.95, respectively (Fig. 3G), indicating effective enrichment even at low target cell concentrations. While sample purity was not maximized under the current operating conditions, the use of 100 : 200 (sample : buffer) flow rate ratio, which was selected based on the prior evidence supporting optimal recovery,[28,30,34] enabled robust capture of rare cells. This trade-off reflects a deliberate design choice prioritizing sensitivity, which is critical in applications where maximizing target cell yield is critical. Future optimization of flow parameters may further enhance purity without compromising recovery.

Evaluation of cancer cell isolation using EasySep™

We assessed the recovery performance of the EasySep™ system using spike-in experiments with PANC1 cells in PBS, lysed blood, and whole blood. Recovered cells were enumerated under the microscope following the complete EasySep™ protocol (Fig. 4A). Although the EasySep™ protocol does not require RBC lysis, we included both lysed and whole blood conditions to evaluate the impact of RBC depletion on recovery performance. When whole blood was used directly, cell recovery rates were low, 3.8 ± 0.2%, 4.6 ± 1%, and 3.3 ± 0.4% for 50, 100, and 500 cells per mL spikes, respectively (Fig. 4B). The high cell density in whole blood hindered sample handling and likely contributed to reduced recovery. Slightly improved recovery was observed in lysed blood samples, with mean values of 4.6 ± 3%, 5.3 ± 2.1%, and 8.3 ± 1% for the same spike concentrations. PBS samples yielded the highest recovery rates, with 6.5 ± 0.9%, 7 ± 1.4%, and 10 ± 1%, respectively. These results suggest that sample complexity significantly affects EasySep™ performance, with minimal interference from blood cell contamination in PBS.

It is important to note that recovery was assessed after the full EasySep™ workflow, including magnetic separation, centrifugation, and elution—each of which may contribute to cumulative cell loss. At a higher spike concentration of 10^4 cells per mL in lysed blood, recovery increased to 13.8 ± 1.1%. These results are comparable to findings by Drucker *et al.*,[12] who reported a mean recovery of 24 ± 19% using a combination of EpCAM Positive Selection Kit and CD45 Depletion Kit. The higher recovery in that study may be attributed to the dual-kit approach, whereas our experiments used only the CD45 Depletion Kit. Due to the low recovery rates, cytocentrifugation was omitted to prevent further loss. Instead, recovered cells were directly transferred to glass slides for enumeration. Blood cell contamination remained evident in both whole and lysed blood samples, and PANC1 cells were identified *via* nuclear staining, which could be

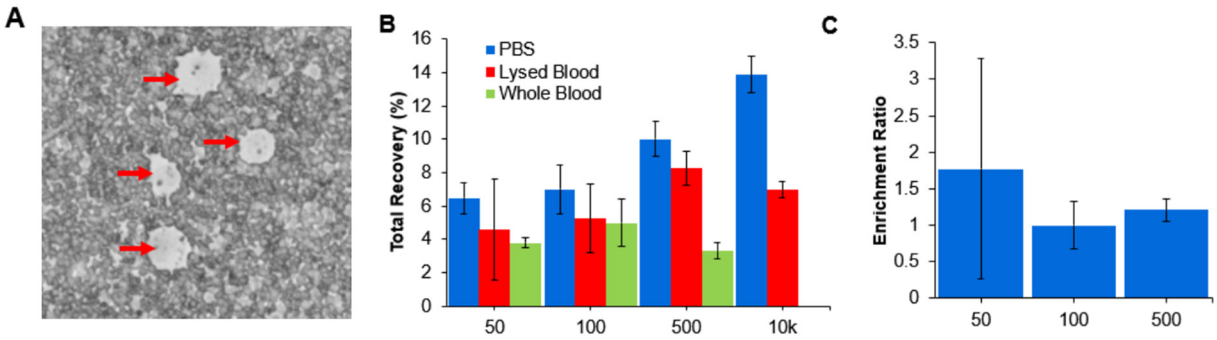

Fig. 4 Recovery and enrichment performance of EasySep™ immunomagnetic isolation. A) Representative image of PANC1 cells recovered using EasySep™, indicated by red arrows. B) Total recovery of PANC1 cells at varying spike-in concentrations in PBS, lysed blood, and whole blood, illustrating the impact of sample matrix on recovery efficiency. C) Enrichment ratios following EasySep™ separation across different spike-in concentrations, reflecting the method's ability to deplete background cells and concentrate target cells.

obscured by background cells. The resulting enrichment ratios were modest—approximately 1.0 to 1.8—reflecting both low recovery and limited purity (Fig. 4C).

Despite these limitations, EasySep™ was able to isolate a detectable number of tumor cells, and performance may be enhanced through integration with positive selection strategies. For example, combining EasySep™ with microfluidic positive selection has yielded recovery rates of 33–82%.[26] EasySep™ technologies have also demonstrated higher efficiency in peripheral blood mononuclear cell (PBMC) isolation for applications such as single-cell transcriptomics and immune profiling.[35,36] However, for rare cell isolation, our iMF platform achieved up to ~8-fold higher recovery and ~5-fold greater enrichment compared to EasySep™, highlighting its superior performance. Our platform also offers significant procedural advantages over the EasySep™ system by reducing manual handling steps and thus minimizing user-induced errors, lowering the risk of cell loss, and improving reproducibility. Additionally, the reduced reagent requirements translate to lower per-sample operational costs. Although the processing time is inherently linked to flow rate throughput (10 min per 1 mL of sample), this limitation can be effectively addressed by parallelizing multiple units, enabling scalability and throughput optimization. In contrast, EasySep™ operates with a fixed runtime of approximately 65 min per run, offering less flexibility in high-throughput settings.

CTC detection from pancreatic cancer patients

To assess the clinical applicability of the isolation methods, we evaluated their performance in separating CTCs and CECs from patient blood samples. CTCs have been identified across all stages of PDAC, including pre-malignant conditions. Evidence suggests that epithelial cell migration and intravasation into the bloodstream can occur early in pancreatic cancer progression. In pre-malignant stages, such as those involving intraductal papillary mucinous neoplasms (IPMNs), these cells are referred to as CECs,[9] and have been detected in up to 88% of patients. This highlights their potential utility in early detection and risk assessment.[5] Therefore, the ability to reliably isolate CTCs and CECs is critical for improving our understanding of disease recurrence, evaluating therapeutic interventions, and ultimately enhancing clinical outcomes.

To validate the isolation methods in a clinical context, we collected blood samples from surgical patients diagnosed with PDAC, NET, or IPMN. Samples were obtained pre-operatively, intra-operatively, and post-operatively (at 24 and 72 hours). Pre-operative and 72 hour post-operative samples were drawn from the forearm, while intra-operative and 24 hour post-operative samples were collected from an arterial line. To enhance the separation performance of the iMF device, we used a slightly longer microchannel (150 μm × 50 μm × 30 mm, $w \times h \times l$). Because the channel cross-section and flow rate were held constant, the resulting change in cut-off size due to increased channel length was minimal, less than 1 μm, and effectively negligible given the deformability of cells. In contrast, the extended channel length substantially improved sorting efficiency, achieving values exceeding 90%.[30] This design modification enhanced the discrimination of target cells, further supporting the clinical utility of the platform. The blood volume was aliquoted into two parts and processed using either our iMF device or the EasySep™ system. To identify CTCs and CECs following separation, we used immunofluorescent staining based on established marker profiles. While previous studies have used combinations such as EpCAM+/CK+/CD45−[37] or vascular endothelial cadherin (VE-cad+)/CD45−[38] to distinguish these cell types, we adopted a CK+/CD45− staining strategy for identification. Specifically, CECs were identified in IPMN samples, and CTCs were identified in PDAC and NET samples based on cytokeratin (CK) positivity and absence of CD45 expression. WBCs were excluded based on CD45+ staining.

To directly compare the performance of the iMF and EasySep™ systems, both methods were applied to the first 3 out of 6 patient blood samples. In patient A, who was diagnosed with IPMN, we detected CECs in the intra-operative blood sample using the iMF device, with an estimated concentration of 390 CECs per mL. In contrast, the EasySep™ system detected only approximately 14 CECs per mL from the same sample across all analyzed slides (Fig. 5A and B). The average diameter of the CECs was 11.9 μm. Patient B, also diagnosed with IPMN but without evidence of carcinoma, showed no detectable CECs in either system. Similarly, patient C, who was diagnosed with NET, had no detectable CTCs in the analyzed samples.

Based on the superior performance observed in initial comparisons, the iMF device was used exclusively for processing the remaining patient samples. CTCs were detected in all cases, with estimated concentrations of 189,

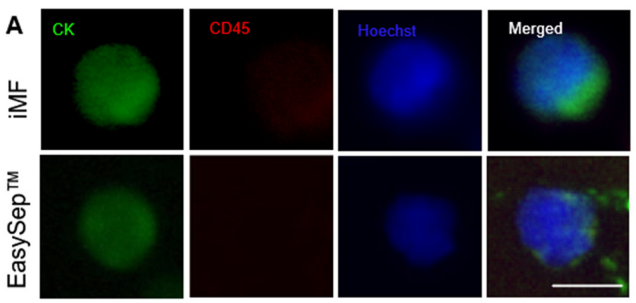

B

	iMF (per mL)	EasySep™ (per mL)
Patient A (IPMN)	390	14
Patient B (IPMN)	0	0
Patient C (NET)	0	0

Fig. 5 Comparison of isolation platforms using patient blood samples. A) Representative images of CECs isolated from patients diagnosed with NET and IPMN. B) Quantification of CECs recovered from patient blood samples using each isolation method. Scale bar is 10 μm.

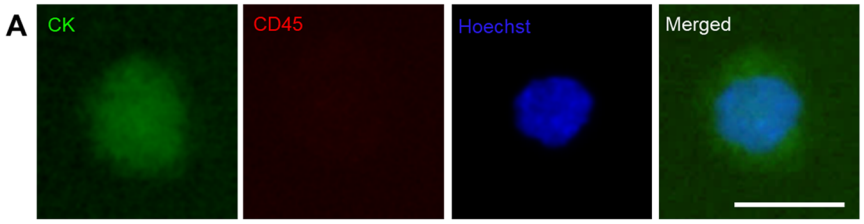

B

PDAC Patient	Avg. # CTCs detected (per mL)	Average Size (μm)
Patient D (w/ chemo)	189	10.9 ± 2.2
Patient E (no chemo)	28	18.9 ± 1.0
Patient F (w/ chemo)	37	13.8 ± 0.8

Fig. 6 Recovery of CTCs from patient blood samples. A) Representative fluorescence images of isolated CTCs (CK+/CD45–) from patients with PDAC. B) Quantification of CTCs recovered from patient blood samples, averaged across all time points. Scale bar, 20 μm.

28, and 37 CTCs per mL in patients D, E, and F, respectively. These values fall within the range reported in previous studies across various stages of PDAC.[15] The average size of CTCs across all time points was 10.9 ± 2.2 μm for patient D, 18.9 ± 1.0 μm for patient E, and 13.8 ± 0.8 μm for patient F (Fig. 6B). No significant variation in cell size was observed between surgical time points. Notably, patients D and F, both of whom had residual PDAC and received chemotherapy, exhibited smaller CTCs compared to patient E, who had an IPMN that progressed to PDAC and did not receive chemotherapy. These findings suggest that both disease stage and treatment history may influence the size and abundance of CTCs. Notably, CTCs exhibit considerable size variability and may fall below the device's cutoff threshold, as observed in Patient D. Although extending the device length improves capture efficiency, it cannot fully compensate for this intrinsic heterogeneity. Consequently, while WBC depletion enhances sample purity, it remains incomplete, resulting in residual leukocyte contamination. To quantify both WBC depletion and overall sample purity, we evaluated the enrichment ratio in our spike-in experiments.

In all three patients, post-operative samples contained more CTCs than pre-operative and intra-operative samples, although the differences were not statistically significant. The most pronounced increase was observed between intra-operative and 72 hour post-operative time points (Fig. 7). This trend supports the hypothesis that surgical manipulation of the tumor may lead to increased CTC release into circulation.[3,39] Similar observations have been reported in other studies, which noted elevated levels of tumor-associated analytes and rare cells in peripheral blood following surgical resection.[39]

It is important to acknowledge that blood collection sites varied across time points (peripheral vein *vs.* arterial line), which may influence CTC counts. Additionally, the small sample size limits the extent to which these findings can be generalized. Further studies with larger cohorts are needed to clarify the effects of chemotherapy on CTC size and abundance. Nonetheless, prior research has demonstrated that chemotherapy can reduce tumor burden,[40] which may partially explain the observed differences.

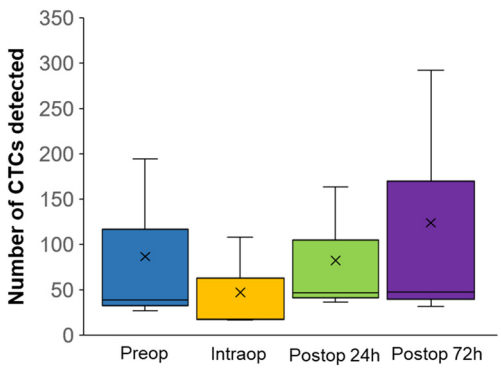

Fig. 7 Distribution of CTCs across surgical time points. Quantification of CTCs isolated from patients with PDAC at pre-operative, intra-operative, and post-operative (24 h and 72 h) time points. Data reflect dynamic changes in CTC levels associated with surgical intervention.

Conclusions

In this study, we conducted a rigorous, side-by-side comparison of a size-based inertial microfluidic system and an immunomagnetic negative selection method (EasySep™) for isolating pancreatic tumor cells from human blood samples. Both approaches enabled the recovery of label-free cancer cells, preserving phenotypic heterogeneity of CTCs and CECs across various stages of pancreatic disease, including PDAC, IPMN, and NET. Here, we implemented a directly comparable evaluation of our microfluidic device with a widely used conventional isolation method. We explicitly designed our study to benchmark performance under matched experimental conditions, including identical sample sources, spike-in protocols, and operator handling. Our findings demonstrate that the iMF system achieves up to an ~8-fold higher recovery and a ~5-fold greater enrichment ratio compared to EasySep™, particularly at low cell concentrations. The reduced recovery observed with EasySep™ is likely due to cell loss during multiple sample handling and transfer steps.

While the iMF system demonstrated superior performance compared to the conventional method, further optimization is needed to enhance both recovery and purity. A major contributor to limited recovery is cytocentrifugation, which is currently required for downstream phenotypic analysis and accounts for approximately 50% cell loss. As a result, overall recovery is constrained to ~44%. This underscores a clear opportunity to refine the workflow in order to improve yield without compromising cell integrity.

Importantly, our findings underscore the clinical potential of the iMF system. In patients with IPMN, the platform achieved a 27-fold higher detection of CECs compared to EasySep™, suggesting its utility in identifying early indicators of malignant transformation. Additionally, CTCs were successfully isolated from PDAC patients undergoing surgical resection, with a modest post-operative increase in CTC counts, consistent with prior reports of surgery-induced tumor cell dissemination. These observations support the use of microfluidic isolation to gain insights into tumor biology and disease dynamics.

Liquid biopsy approaches such as this offer a minimally invasive means to detect and monitor tumor-derived cells across the spectrum of pancreatic disease. The integration of our iMF system into clinical workflows holds promise for improving prognostic assessments, guiding therapeutic decisions, and advancing our understanding of disease progression. Further clinical studies are needed to characterize the phenotypic diversity of pancreatic CTCs and CECs and to refine detection strategies for broader clinical application.

Conflicts of interest

There are no conflicts to declare.

Data availability

The data that support the findings of this study are available within this article. Data collected from human participants are not available for confidentiality reasons.

Acknowledgements

This work is supported by the American Society of Regional Anesthesia and Pain Medicine, UIC COVID-19 Faculty Research Relief Program, and the UIC College of Engineering GPIP program.

References

1 V. Martini, S. Timme-Bronsert, S. Fichtner-Feigl, J. Hoeppner and B. Kulemann, Circulating Tumor Cells in Pancreatic Cancer: Current Perspectives, *Cancers*, 2019, **11**(11), 1659.
2 J. Werner, S. E. Combs, C. Springfeld, W. Hartwig, T. Hackert and M. W. Büchler, Advanced-stage pancreatic cancer: therapy options, *Nat. Rev. Clin. Oncol.*, 2013, **10**(6), 323–333.
3 S. Tohme, R. L. Simmons and A. Tsung, Surgery for Cancer: A Trigger for Metastases, *Cancer Res.*, 2017, **77**(7), 1548–1552.
4 F. C. Bidard, F. Huguet, C. Louvet, L. Mineur, O. Bouché and B. Chibaudel, *et al.*, Circulating tumor cells in locally advanced pancreatic adenocarcinoma: the ancillary CirCe 07 study to the LAP 07 trial, *Ann. Oncol.*, 2013, **24**(8), 2057–2061.
5 D. Yeo, A. Bastian, H. Strauss, P. Saxena, P. Grimison and J. E. J. Rasko, Exploring the Clinical Utility of Pancreatic Cancer Circulating Tumor Cells, *Int. J. Mol. Sci.*, 2022, **23**(3), 1671.
6 T. Kurihara, T. Itoi, A. Sofuni, F. Itokawa, T. Tsuchiya and S. Tsuji, *et al.*, Detection of circulating tumor cells in patients with pancreatic cancer: a preliminary result, *J. Hepatobiliary Pancreat. Surg.*, 2008, **15**(2), 189–195.
7 A. De Albuquerque, I. Kubisch, G. Breier, G. Stamminger, N. Fersis and A. Eichler, *et al.*, Multimarker Gene Analysis of Circulating Tumor Cells in Pancreatic Cancer Patients: A Feasibility Study, *Oncology*, 2012, **82**(1), 3–10.
8 A. D. Rhim, F. I. Thege, S. M. Santana, T. B. Lannin, T. N. Saha and S. Tsai, *et al.*, Detection of Circulating Pancreas Epithelial Cells in Patients With Pancreatic Cystic Lesions, *Gastroenterology*, 2014, **146**(3), 647–651.
9 A. D. Rhim, E. T. Mirek, N. M. Aiello, A. Maitra, J. M. Bailey and F. McAllister, *et al.*, EMT and Dissemination Precede Pancreatic Tumor Formation, *Cell*, 2012, **148**(1–2), 349–361.
10 A. J. Rushton, G. Nteliopoulos, J. A. Shaw and R. C. Coombes, A Review of Circulating Tumour Cell Enrichment Technologies, *Cancers*, 2021, **13**(5), 970.
11 C. Macaraniag, Q. Luan, J. Zhou and I. Papautsky, Microfluidic techniques for isolation, formation, and characterization of circulating tumor cells and clusters, *APL Bioeng.*, 2022, **6**(3), 031501.
12 A. Drucker, E. M. Teh, R. Kostyleva, D. Rayson, S. Douglas and D. M. Pinto, Comparative performance of different methods for circulating tumor cell enrichment in metastatic breast cancer patients, *PLoS One*, 2020, **15**(8), e0237308.
13 S. Nagrath, R. M. Jack, V. Sahai and D. M. Simeone, Opportunities and Challenges for Pancreatic Circulating Tumor Cells, *Gastroenterology*, 2016, **151**(3), 412–426.
14 T. Wei, X. Zhang, Q. Zhang, J. Yang, Q. Chen and J. Wang, *et al.*, Vimentin-positive circulating tumor cells as a biomarker for diagnosis and treatment monitoring in patients with pancreatic cancer, *Cancer Lett.*, 2019, **452**, 237–243.
15 J. Tang, Q. Zheng, Q. Wang, Y. Zhao, P. Ananthanarayanan and C. Reina, *et al.*, CTC-derived pancreatic cancer models serve as research tools and are suitable for precision medicine approaches, *Cell Rep. Med.*, 2024, 101692.
16 J. Zhou, P. Mukherjee, H. Gao, Q. Luan and I. Papautsky, Label-free microfluidic sorting of microparticles, *APL Bioeng.*, 2019, **3**(4), 041504.
17 D. R. Gossett, W. M. Weaver, A. J. Mach, S. C. Hur, H. T. K. Tse and W. Lee, *et al.*, Label-free cell separation and sorting in microfluidic systems, *Anal. Bioanal. Chem.*, 2010, **397**(8), 3249–3267.

18 F. I. Thege, T. B. Lannin, T. N. Saha, S. Tsai, M. L. Kochman and M. A. Hollingsworth, *et al.*, Microfluidic immunocapture of circulating pancreatic cells using parallel EpCAM and MUC1 capture: characterization, optimization and downstream analysis, *Lab Chip*, 2014, **14**(10), 1775–1784.

19 M. C. Miller, P. S. Robinson, C. Wagner and D. J. O'Shannessy, The Parsortix™ Cell Separation System—A versatile liquid biopsy platform, *Cytometry, Part A*, 2018, **93**(12), 1234–1239.

20 M. Ciccioli, K. Kim, N. Khazan, J. D. Khoury, M. J. Cooke and M. C. Miller, *et al.*, Identification of circulating tumor cells captured by the FDA-cleared Parsortix® PC1 system from the peripheral blood of metastatic breast cancer patients using immunofluorescence and cytopathological evaluations, *J. Exp. Clin. Cancer Res.*, 2024, **43**, 240.

21 E. Sollier-Christen, C. Renier, T. Kaplan, E. Kfir and S. C. Crouse, VTX-1 Liquid Biopsy System for Fully-Automated and Label-Free Isolation of Circulating Tumor Cells with Automated Enumeration by BioView Platform, *Cytometry, Part A*, 2018, **93**(12), 1240–1245.

22 Y. Lee, G. Guan and A. A. Bhagat, ClearCell® FX, a label-free microfluidics technology for enrichment of viable circulating tumor cells, *Cytometry, Part A*, 2018, **93**(12), 1251–1254.

23 E. Lin, L. Rivera-Báez, S. Fouladdel, H. J. Yoon, S. Guthrie and J. Wieger, *et al.*, High-Throughput Microfluidic Labyrinth for the Label-free Isolation of Circulating Tumor Cells, *Cell Syst.*, 2017, **5**(3), 295–304.e4.

24 M. Yu, A. Bardia, N. Aceto, F. Bersani, M. W. Madden and M. C. Donaldson, *et al.*, Ex vivo culture of circulating breast tumor cells for individualized testing of drug susceptibility, *Science*, 2014, **345**(6193), 216–220.

25 K. Chen, J. Amontree, J. Varillas, J. Zhang, T. J. George and Z. H. Fan, Incorporation of lateral microfiltration with immunoaffinity for enhancing the capture efficiency of rare cells, *Sci. Rep.*, 2020, **10**(1), 14210.

26 J. Cha, H. Cho, J. S. Chung, J. S. Park and K. H. Han, Effective Circulating Tumor Cell Isolation Using Epithelial and Mesenchymal Markers in Prostate and Pancreatic Cancer Patients, *Cancers*, 2023, **15**(10), 2825.

27 M. Zeinali, V. Murlidhar, S. Fouladdel, S. Shao, L. Zhao and H. Cameron, *et al.*, Profiling Heterogeneous Circulating Tumor Cells (CTC) Populations in Pancreatic Cancer Using a Serial Microfluidic CTC Carpet Chip, *Adv. Biosyst.*, 2018, **2**(12), 1800228.

28 J. Zhou, A. Kulasinghe, A. Bogseth, K. O'Byrne, C. Punyadeera and I. Papautsky, Isolation of circulating tumor cells in non-small-cell-lung-cancer patients using a multi-flow microfluidic channel, *Microsyst. Nanoeng.*, 2019, **5**(1), 8.

29 P. Mukherjee, F. Nebuloni, H. Gao, J. Zhou and I. Papautsky, Rapid Prototyping of Soft Lithography Masters for Microfluidic Devices Using Dry Film Photoresist in a Non-Cleanroom Setting, *Micromachines*, 2019, **10**(3), 192.

30 C. Macaraniag, J. Zhou, N. Hay, I. Papautsky, J. Li and W. Putzbach, Microfluidic isolation of breast cancer circulating tumor cells from microvolumes of mouse blood, *Electrophoresis*, 2023, **44**, 1859–1867.

31 J. Zhou, P. V. Giridhar, S. Kasper and I. Papautsky, Modulation of rotation-induced lift force for cell filtration in a low aspect ratio microchannel, *Biomicrofluidics*, 2014, **8**(4), 044112.

32 A. G. J. Tibbe, M. C. Miller and L. W. M. M. Terstappen, Statistical considerations for enumeration of circulating tumor cells, *Cytometry, Part A*, 2007, **71**(3), 154–162.

33 M. Yu, D. T. Ting, S. L. Stott, B. S. Wittner, F. Ozsolak and S. Paul, *et al.*, RNA sequencing of pancreatic circulating tumour cells implicates WNT signalling in metastasis, *Nature*, 2012, **487**(7408), 510–513.

34 A. Bogseth, J. Zhou and I. Papautsky, Evaluation of Performance and Tunability of a Co-Flow Inertial Microfluidic Device, *Micromachines*, 2020, **11**(3), 287.

35 R. Hanamsagar, T. Reizis, M. Chamberlain, R. Marcus, F. O. Nestle and E. De Rinaldis, *et al.*, An optimized workflow for single-cell transcriptomics and repertoire profiling of purified lymphocytes from clinical samples, *Sci. Rep.*, 2020, **10**(1), 2219.

36 G. S. Marques, Z. Silva and P. A. Videira, Antitumor Efficacy of Human Monocyte-Derived Dendritic Cells: Comparing Effects of two Monocyte Isolation Methods, *Biol. Proced. Online*, 2018, **20**(1), 4.

37 J. W. Franses, O. Basar, A. Kadayifci, O. Yuksel, M. Choz and A. S. Kulkarni, *et al.*, Improved Detection of Circulating Epithelial Cells in Patients with Intraductal Papillary Mucinous Neoplasms, *Oncologist*, 2018, **23**(1), 121–127.

38 J. W. Po, A. Roohullah, D. Lynch, A. DeFazio, M. Harrison and P. R. Harnett, *et al.*, Improved ovarian cancer EMT-CTC isolation by immunomagnetic targeting of epithelial EpCAM and mesenchymal N-cadherin, *J. Circ. Biomarkers*, 2018, **7**, 184945441878261.

39 S. N. Shishido, E. Lin, N. Nissen, G. Courcoubetis, D. Suresh and J. Mason, *et al.*, Cancer-related cells and oncosomes in the liquid biopsy of pancreatic cancer patients undergoing surgery, *npj Precis. Oncol.*, 2024, **8**(1), 36.

40 V. Kunzmann, R. K. Ramanathan, D. Goldstein, H. Liu, S. Ferrara and B. Lu, *et al.*, Tumor Reduction in Primary and Metastatic Pancreatic Cancer Lesions With nab-Paclitaxel and Gemcitabine: An Exploratory Analysis From a Phase 3 Study, *Pancreas*, 2017, **46**(2), 203–208.

